Applied Physics Letters

PLEASE CITE THIS ARTICLE AS DOI: 10.1063/5.0058685

AIP Publishing

Discarded gems: Thermoelectric performance of materials with band gap emerging at the hybrid-functional level

Kristian Berland,[1, a)] Ole Martin Løvvik,[2, 3] and Rasmus Tranås[1]

[1)] *Department of Mechanical Engineering and Technology Management, Norwegian University of Life Sciences, NO-1432 Ås, Norway.*

[2)] *SINTEF Industry, NO–0314 Oslo, Norway*

[3)] *Centre for Materials Science and Nanotechnology, Department of Physics, University of Oslo, NO-0316 Oslo, Norway*

(Dated: July 19, 2021)

A finite electronic band gap is a standard filter in high-throughput screening of materials using density functional theory (DFT). However, because of the systematic underestimation of band gaps in standard DFT approximations, a number of compounds may incorrectly be predicted metallic. In a more accurate treatment, such materials may instead appear as low band gap materials and could e.g. have good thermoelectric properties if suitable doping is feasible. To explore this possibility, we performed hybrid functional calculations on 1093 cubic materials listed in the MaterialsProjects database with four atoms in the primitive unit cell, spin-neutral ground state, and a formation energy within 0.3 eV of the convex hull. Out of these materials, we identified eight compounds for which a finite band gap emerges. Evaluating electronic and thermal transport properties of these compounds, we found the compositions $MgSc_2Hg$ and Li_2CaSi to exhibit promising thermoelectric properties. These findings underline the potential of reassessing band gaps and band structures of compounds to indentify additional potential thermoelectric materials.

Thermoelectrics, with their ability to turn temperature gradients into electricity, can contribute to making the transition into a green economy with reduced greenhouse emission by recovering some of the waste heat generated in various industrial processes.[1–3] While thermoelectric materials have traditionally not been sufficiently efficient for this task, great strides forward have been made in recent years. This has in turn intensified the hunt for novel thermoelectric materials,[4–10] including the adoption of high-throughput screening and material informatics[11,12] approaches.

The thermoelectric figure-of-merit $ZT = \sigma S^2 T/(\kappa_e + \kappa_\ell)$, which is measure of the conversion efficacy, is given by the conductivity σ, the Seebeck coefficient S, the electronic κ_e, and lattice thermal κ_ℓ conductivity. Among these, all but κ_ℓ are strongly linked to the electronic band structure. The electronic band gap $E_{\rm gap}$ is a particularly important parameter, determining the temperature for the onset of minority carrier transport, which causes a marked drop in S. It also has an indirect influence on the band curvature, i.e. as revealed by $\mathbf{k}\cdot\mathbf{p}$-theory.[13] Following Sofo and Mahan,[14] a band gap of approximately 6-10 $k_{\rm B}T$ has traditionally been considered attractive. However, their analysis was based on a direct band-gap model with a single valley. Given its link to the band curvature, the band gap $E_{\rm gap}$ can also be viewed as a scale factor making a low band gap material more prone to exhibit multiple valleys in multipocketed band structures;[15] nonetheless, the need to limit bipolar transport has made the existence of a finite band gap a standard criterion in most screening studies.[7] Recently, attention has been broadened to other types of materials: Semi-metals with a strong asymmetry between conduction and valence bands have e.g. been marked as potential thermoelectric materials.[16,17] Gapped metallic systems, which possess a band gap within the conduction or valence band, could also potentially exhibit good thermoelectric properties, once the band edge is sufficiently doped towards the Fermi level.[18]

A completely different reason for not discarding predicted metallic systems is that a number of them might have been mislabeled due to various approximations used in density functional theory (DFT).[19] In particular, the commonly used generalized gradient approximation (GGA) systematically underestimates band gaps.[20,21] This is less the case for hybrid functionals,[22] which mix a fraction of "exact" Fock exchange with the GGA.[23,24] In the empirical linear relations between experimental and computed band gaps of Morales-García et al.,[21] the offset of about 0.92 eV roughly indicates that compounds with a band gap smaller than this are likely to be incorrectly predicted as metallic by GGA.

In this work, we computed the band gap of 1093 cubic nonmagnetic materials listed in the Materials Project database[25] with four atoms in the primitive unit cell and a formation energy within 0.3 eV of the convex hull. These compounds include the full Heusler compounds with spacegroup $Fm\bar{3}m$, inverse Heuslers with spacegroup $F\bar{4}3m$ (both with composition X_2YZ) and binary AB_3 compounds. This reassessment resulted in eight compounds that were possibly mislabeled metallic by GGA. DFT calculations were performed using the VASP[26–29] software package. The consistent-exchange van der Waals functional vdW-DF-cx functional[30,31] was used for obtaining relaxed crystal structures and lattice thermal conductivities. While mostly used for modelling

---

[a)] Electronic mail: kristian.berland@nmbu.no

compound	#valence	E_{hull} (MP)	band gap (eV)
$AlVFe_2$	24	0	0.78
Ba_2HgPb	20	0	0.06
$HfSnRu_2$	24	0	0.21
Li_2CaSi	10	0	0.01
$MgSc_2Hg$	20	0	0.23
$TaInRu_2$	24	0	0.05
$TiSiOs_2$	24	0	0.55
$VGaFe_2$	24	0	0.66

Table I. Properties of new band-gap compounds

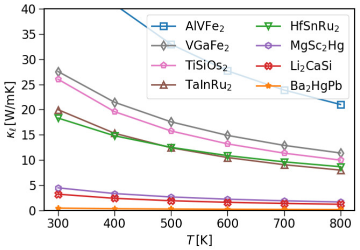

Figure 1. Lattice thermal conductivity of identified compounds computed with TDEP.

non-covalently bonded solids, recent studies have shown that vdW-DF-cx can improve structure and energetics compared to that of GGA of ionic and covalently-bonded structures as well.[32–34] To identify materials that could possess a band gap at the hybrid level, we first computed the band gap using merely a $4 \times 4 \times 4$ **k**-sampling of the Brillouin zone including spin-orbit coupling using the HSE06[23,35] hybrid functional. Such a low sampling can result in inaccurate Kohn-Sham energies and we acknowledge that there is a slight risk that some compounds with very low band gap are missed. But generally, the coarse sampling will cause a few systems to incorrectly appear with a finite or too large band gap. All systems with a finite band gap in the first stage were therefore reassessed with a $12 \times 12 \times 12$ **k**- Brillouin-zone sampling of the Fock operator and charge density, which is used to compute the band structure path using 101 **k**-points along W-L-Γ-X-K to obtain an accurate band gap. For the new band-gap compounds, the electronic transport properties were computed with the Boltzmann Transport equation in the constant relaxation time approximation with $\tau = 10^{-14}$s using BoltzTraP.[36] To ensure dense grid sampling, we used a corrected $\mathbf{k} \cdot \mathbf{p}$-based interpolation method,[37,38] using the same computational parameters as in Ref. 39 The lattice thermal conductivity, κ_ℓ, was computed using the temperature-dependent effective potential (TDEP) method.[40,41] A canonical ensemble was used to generate 50 uncorrelated configurations based on a $3 \times 3 \times 3$ repetition of the relaxed primitive cell.[42] The positions and forces of the supercells allowed for extraction of second- and third-order force constants. The cutoff for the second-order interactions was set to 7 Å, while to third-order, a cutoff slightly larger than half the width of the supercell was used. Reciprocal space discretization for Brillouin zone integrations was done using a $35 \times 35 \times 35$ **q**-point grid. Isotope scattering was also included. All supplementary GGA calculations in this letter were based on the version of Perdew-Burke-Ernzerhof (PBE).[43]

Among the 1093 compounds materials examined, eight compounds have a band gap at the HSE06 level as listed in Tab. I, corresponding band structures are provided in supplementary material (SM).

Figure 1 shows the computed κ_ℓ for the identified compounds. Very low values of κ_ℓ was found for Ba_2HgPb ranging from 0.46 W/mK at 300 K to 0.17 W/mK at 800 K. This compound was also studied by He et al.[44] predicting values of κ_ℓ somewhat larger than ours. Possible reasons for this differene inlude their use of a compressive sensing lattice dynamic technique[45] to obtain third-order force constants and other technical detials, differing exchange correlation functionals, and the phonon-mode renormalization inherit to TDEP. Comparing TDEP and Phonopy, Feng et al.[46] found lower κ_ℓ for TDEP than with the standard-finite difference approach and argued that TDEP is better suited to describe low-κ_ℓ materials.

Based solely on Fig. 1, only Ba_2HgPb, Li_2CaSi, and $MgSc_2Hg$ have low enough κ_ℓ to conceivably be good thermoelectric materials. Yet, the literature is riddled with examples of how various disorder-related scattering mechanisms such as grain boundaries, defects, and substitutions can dramatically lower κ_ℓ.[47–54] For this reason, we used $\kappa_\ell = 4$ W/mK as the maximum for all materials in further comparisons.

Figure 2 plot the optimal doping concentration against peak ZT for each of the compounds in temperature steps of 100 K from 300 K to 800 K, for doping concentration between $10^{18}\mathrm{cm}^{-3}$ and $3 \times 10^{21}\mathrm{cm}^{-3}$. Based on this plot, we deem Li_2CaSi and $MgSc_2Hg$ to have great potential as thermoelectric n-type materials, while $MgSc_2Hg$ and $AlVFe_2$ have some potential as p-type thermoelectrics. n-type $AlVFe_2$ has been studied earlier theoretically at the hybrid functional level,[55] and experimentally.[56,57] The study of Mikami et al.[56] measured ZT in a similar range as us once doping and sublattice disorder were introduced. While Li_2CaSi is reported as stable in the $Fm\bar{3}m$ Heusler phase in the Materials Project; experimentally, it has been crystallized in the orthorhombic $Pmmm$ phase.[58] The related Li_2CaSn, on the other hand, does crystallize in the Heusler phase. No experimental realizations of $MgSc_2Hg$ are known to us.

The origin of the high ZT of Li_2CaSi and $MgSc_2Hg$ can be related to their band structures as shown in Fig. 3. The band structure of Li_2CaSi exhibits some noticeable features: *i.* Dirac points at the Γ-point with a band opening of 0.01 eV, *ii.* near convergence of a number

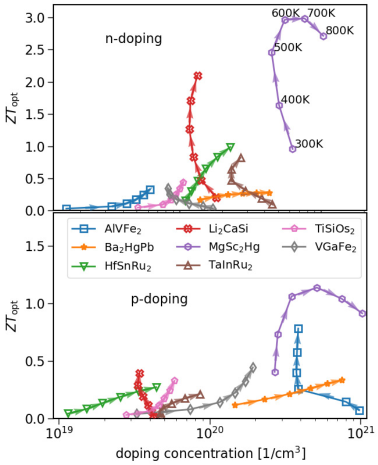

Figure 2. Optimized ZT at different temperatures from 300 K to 800 K with arrows indicating increasing temperature in steps of 100 K. The vertical axis gives the optimized ZT while the horizontal gives the corresponding doping concentration.

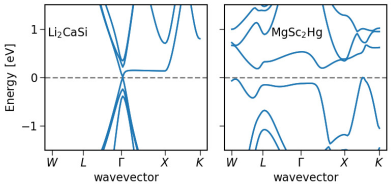

Figure 3. Electronic band structures of Li$_2$CaSi and MgSc$_2$Hg.

of additional bands at the Γ point, *iii.* electron bands that are flat in the Γ-X direction, but dispersive in the X-K direction. In our study, we find similar features in the band structure of HfSnRu$_2$ and TaInRu$_2$, which also exhibit relatively high ZT for n-type doping. While Bilc et al.[55] argued that band structures of this type can give rise to high ZT due to the their effectively low-dimensional transport, Park et al.[59] demonstrated that flat-and-dispersive band structures, specifically for the case of Fe$_2$TiSi, can cause large effective scattering phase-space which significantly reduces the power factor. In contrast, MgSc$_2$Hg band structure has a multi-valley structure in particular in the conduction band. In fact, with the exception of the highly dispersive band in the X-point, the band structure can be viewed as a partial realization of δ-function like transport spectral function, which in the analysis of Mahan and Sofo is optimal for thermoelectric performance.[60] Other cubic structures, such as the 10-valence electron full-Heusler compounds predicted by He et al.[61] also have similarly attractive band structure features.

Figure 4a shows Pisarenko-type plots for the thermoelectric properties of MgSc$_2$Hg at 300, 600, and 800 K. while 4b shows the underlying spectral quantities giving rise to these properties. They are related to through the transport spectral function $\Sigma(\epsilon)$ as follows[36]

$$\sigma = e^2 \int \mathrm{d}\epsilon\, \Sigma(\epsilon - \mu_F) f_1(\epsilon - \mu_F) \tag{1}$$

$$\sigma S = (e/T) \int \mathrm{d}\epsilon\, (\epsilon - \mu_{\mathrm{F}}) \Sigma(\epsilon - \mu_F) f_1(\epsilon - \mu_F) \tag{2}$$

$$\kappa_0 = (1/T) \int \mathrm{d}\epsilon\, \Sigma(\epsilon - \mu_F)(\epsilon - \mu_{\mathrm{F}})^2 f_1(\epsilon - \mu_F), \tag{3}$$

where μ_{F} is the Fermi level and f_1 is the Fermi window, given by the derivative of the Fermi-Dirac function, $f_1(\epsilon - \mu_{\mathrm{F}}) = -\mathrm{d}f_{\mathrm{FD}}/\mathrm{d}\epsilon$. The open-circuit electronic thermal conductivity κ_0 is related to the closed-circuit by $\kappa_{\mathrm{e}} = \kappa_0 - T\sigma S^2$. The temperature dependence stems explicitly from the Fermi-Dirac function and implicitly from the temperature dependence of μ_F. A dashed line indicates the peak of $\Sigma(\epsilon)$ for comparison with the band structure in Fig. 3. The figures shows that for MgSc$_2$Hg the magnitude of κ_{e} is a key factor limiting ZT at elevated temperatures. They also show that a minimum in κ_e at 600 and 800 K occurs at a higher doping concentration than what maximises S. They both reach extreme values due to a minimum in the bipolar transport, but the second moment $(\epsilon - \mu_F)^2$ entering into κ_0 (Eq. 3) shifts the optimum of κ_e to a higher doping concentration. The figure also indicates that the rapidly rising $\Sigma(\epsilon)$ up to the peak occurring at 0.55 eV explains why S can be quite large despite a low band gap even at high doping concentrations. At the same time, it shows that this rapid rise is the cause of the large values of κ_e at high temperatures.

Figure 4c and 4d shows corresponding results for Li$_2$CaSi. It is interesting to note that while the band gap is tiny, the low $\Sigma(\epsilon)$ in the valence band makes this compound resemble a wide band-gap semiconductors. In fact, at optimal doping concentration, the bipolar transport occurs almost entirely within the condution band. While the limited bipolar transport results in higher S at lower doping concentrations, Li$_2$CaSi lacks the beneficial peak in $\Sigma(\epsilon)$ present in MgSc$_2$Hg which limits κ_{e} at higher temperatures and doping concentrations. The low band gap of Li$_2$CaSi makes it interesting to also consider the properties of Li$_2$CaSi as predicted at the GGA level. In this case, a finite gap is retained at the Γ -point but the material is self-doped and the flat-and-dispersive band crosses the Fermi level at zero extrinsic doping. An optimal $ZT = 0.76$ at 800 K is predicted – further details in SM.

While we in this study assessed the properties of 1093 four-atom materials using sub-converged hybrid functional calculations, other approaches could also be worth

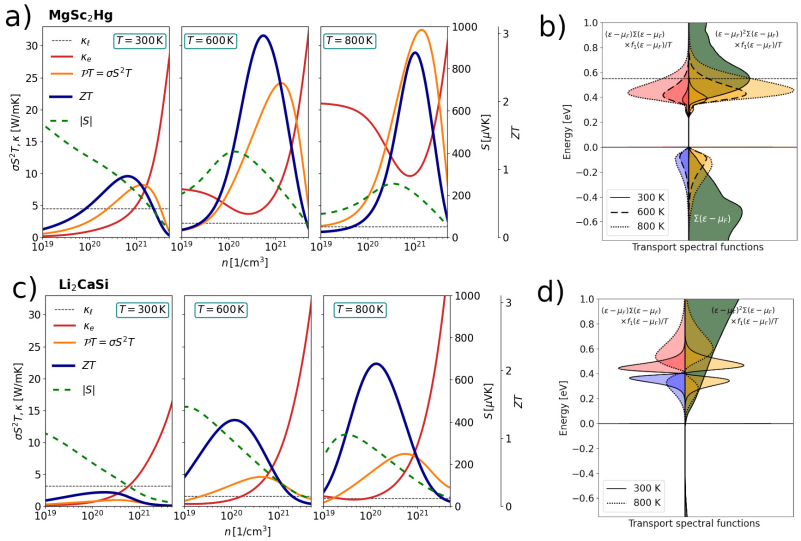

Figure 4. a) [c)] Thermoelectric properties of $MgSc_2Hg$ [Li_2CaSi] as a function of doping doping concentration at 300 K, 600 K, and 800 K. In b) [d)], the green background shows the corresponding transport spectral functions $\Sigma(\epsilon)$. The left and right side of the vertical axis show the spectral contributions to the first and second moment of the $\Sigma(\epsilon)$ weighted by the derivative $f_1(\epsilon) = -\mathrm{d}f_{\mathrm{FD}}(\epsilon)\mathrm{d}\epsilon$, which is proportional to respectively $T\sigma S$ and the closed circuit thermal conductivity κ_0. Results for 600 K omitted for clarity in d)

exploring. We investigated the potential of analyzing the GGA-level density of states, in which a "narrowing" could hint of a finite band gap. Details can be found in the SM. Interestingly, this approach clearly indicated all compounds except the $MgSc_2Hg$ compound; precisely the property that made this material into a promising thermoelectric, i.e. the high density of states close to the band edges at the hybrid level, made the density-of-states narrowing at the GGA-level vanish. We therefore do not generally recommend this approach to uncover high performance thermoelectric materials.

In this letter, we have demonstrated that the use of GGA-level band structures can cause promising thermoelectric materials to be discarded because they are falsely predicted to be metallic. This was illustrated with the finding of new thermoelectric compounds with a band gap appearing at the hybrid functional level: Out of the 1093 studied compounds, 8 were identified with a band gap by hybrid calculations and not by GGA calculations. Out of these, a few were also promising for thermoelectric applications: $MgSc_2Hg$, Li_2CaSi, and to some extent $AlVFe_2$. The Heusler $MgSc_2Hg$ compound, in particular, exhibits excellent potential as a thermoelectric material. We are not aware of any experimental realization of this compound or in-depth stability analysis. Moreover, the toxicity of Hg reduces the attractiveness of this compound for general-purpose applications. In addition to realizability, we stress the use of a constant relaxation-time approximation is a coarse approximation. The inclusion of proper electron-phonon scattering can have a decisive impact upon the power factor and prediced ZT properties.[62] Another concern is whether hybrid functionals in fact do provide accurate band structures for these intermetallic compounds, which can be investigated for instance by performing GW-level calculations, as earlier done for selected Half Heuslers.[63] Despite these caveats, our study clearly underlines that high performing thermoelectric materials can be uncovered through reassessment of electronic band gaps.

On a final note, it is interesting that the three compounds with lowest κ_ℓ and two of the compounds with the highest n-type ZT violated the octet rule or the corresponding 18- and 24-electron rules. This violation is a feature shared with the well-known thermoelectric PbTe and related compounds.[61,64] The existence of lone s-pairs have earlier been linked to low thermal conductivity.[61,65,66] One could speculate that going beyond GGA could be particularly pertinent for the electronic band structure of octet violating systems, similar to what we found earlier for PbTe.[38]

SUPPLEMENTARY MATERIAL

See supplementary material for computed band structures at the HSE06 level, density of states at the PBE level of theory. Band structure and n-type thermoelectric properties of Li_2CaSi

ACKNOWLEDGEMENT

The computations were performed on resources provided by UNINETT Sigma2 - the National Infrastructure for High Performance Computing and Data Storage in Norway. This work is in part funded by the Allotherm project (Project no. 314778) supported by the Research Council of Norway. Additional data beyond what is contained the article and SM are available from the corresponding author upon reasonable request.

REFERENCES

[1] D. M. Rowe and G. Min, “Evaluation of thermoelectric modules for power generation,” J. Power Sources **73**, 193–198 (1998).

[2] M. Dresselhaus, “Overview of thermoelectrics for thermal to electrical energy conversion,” AIP Conf. Proc. **1519**, 36–39 (2013).

[3] G. D. Mahan, “Introduction to thermoelectrics,” APL Materials **4**, 104806 (2016).

[4] S. Bhattacharya and G. K. H. Madsen, “High-throughput exploration of alloying as design strategy for thermoelectrics,” Phys. Rev. B **92** (2015).

[5] S. Bhattacharya and G. K. H. Madsen, “A novel p-type half-Heusler from high-throughput transport and defect calculations,” J. Mater. Chem. C **4**, 11261–11268 (2016).

[6] W. Chen, J.-H. Pöhls, G. Hautier, D. Broberg, S. Bajaj, U. Aydemir, Z. M. Gibbs, H. Zhu, M. Asta, G. J. Snyder, B. Meredig, M. A. White, K. Persson, and A. Jain, “Understanding thermoelectric properties from high-throughput calculations: Trends, insights, and comparisons with experiment,” J. Mater. Chem. C **4**, 4414–4426 (2016).

[7] R. Li, X. Li, L. Xi, J. Yang, D. J. Singh, and W. Zhang, “High-Throughput Screening for Advanced Thermoelectric Materials: Diamond-Like ABX2 Compounds,” ACS Appl. Mater. Interfaces (2019).

[8] C. Barreteau, J.-C. Crivello, J.-M. Joubert, and E. Alleno, “Looking for new thermoelectric materials among TMX intermetallics using high-throughput calculations,” Comput. Mater. Sci. **156**, 96–103 (2019).

[9] L. Chen, H. Tran, R. Batra, C. Kim, and R. Ramprasad, “Machine learning models for the lattice thermal conductivity prediction of inorganic materials,” Comput. Mater. Sci. **170**, 109155 (2019).

[10] Y. Iwasaki, I. Takeuchi, V. Stanev, A. G. Kusne, M. Ishida, A. Kirihara, K. Ihara, R. Sawada, K. Terashima, H. Someya, K.-i. Uchida, E. Saitoh, and S. Yorozu, “Machine-learning guided discovery of a new thermoelectric material,” Sci. Rep. **9**, 2751 (2019).

[11] K. T. Butler, D. W. Davies, H. Cartwright, O. Isayev, and A. Walsh, “Machine learning for molecular and materials science,” Nature **559**, 547 (2018).

[12] J. Hill, G. Mulholland, K. Persson, R. Seshadri, C. Wolverton, and B. Meredig, “Materials science with large-scale data and informatics: Unlocking new opportunities,” MRS Bulletin **41**, 399–409 (2016).

[13] J. M. Luttinger, “Quantum Theory of Cyclotron Resonance in Semiconductors: General Theory,” Phys. Rev. **102**, 1030–1041 (1956).

[14] J. O. Sofo and G. D. Mahan, “Optimum band gap of a thermoelectric material,” Phys. Rev. B **49**, 4565–4570 (1994).

[15] N. Wang, M. Li, H. Xiao, Z. Gao, Z. Liu, X. Zu, S. Li, and L. Qiao, “Band degeneracy enhanced thermoelectric performance in layered oxyselenides by first-principles calculations,” Npj Comput. Mater. **7**, 18 (2021).

[16] M. Markov, X. Hu, H.-C. Liu, N. Liu, S. J. Poon, K. Esfarjani, and M. Zebarjadi, “Semi-metals as potential thermoelectric materials,” Sci. Rep. **8**, 9876 (2018).

[17] M. Markov, S. E. Rezaei, S. N. Sadeghi, K. Esfarjani, and M. Zebarjadi, “Thermoelectric properties of semimetals,” Phys. Rev. Materials **3**, 095401 (2019).

[18] F. Ricci, A. Dunn, A. Jain, G.-M. Rignanese, and G. Hautier, “Gapped metals as thermoelectric materials revealed by high-throughput screening,” J. Mater. Chem. A **8**, 17579–17594 (2020).

[19] O. I. Malyi and A. Zunger, “False metals, real insulators, and degenerate gapped metals,” App. Phys. Rev. **7**, 041310 (2020).

[20] A. Pribram-Jones, D. A. Gross, and K. Burke, “DFT: A Theory Full of Holes?” Annu. Rev. Phys. Chem. **66**, 283–304 (2015).

[21] Á. Morales-García, R. Valero, and F. Illas, “An Empirical, yet Practical Way To Predict the Band Gap in Solids by Using Density Functional Band Structure Calculations,” J. Phys. Chem. **121**, 18862–18866 (2017).

[22] S. Kim, M. Lee, C. Hong, Y. Yoon, H. An, D. Lee, W. Jeong, D. Yoo, Y. Kang, Y. Youn, and S. Han, “A band-gap database for semiconducting inorganic materials calculated with hybrid functional,” Sci Data **7**, 387 (2020).

[23] J. Heyd, G. E. Scuseria, and M. Ernzerhof, “Hybrid functionals based on a screened Coulomb potential,” J. Chem. Phys. **118**, 8207–8215 (2003).

[24] J. Heyd, G. E. Scuseria, and M. Ernzerhof, “Hybrid functionals based on a screened Coulomb potential,” J. Chem. Phys. **118**, 8207–8215 (2003).

[25] A. Jain, S. P. Ong, G. Hautier, W. Chen, W. D. Richards, S. Dacek, S. Cholia, D. Gunter, D. Skinner, G. Ceder, and K. A. Persson, “Commentary: The Materials Project: A materials genome approach to accelerating materials innovation,” APL Materials **1**, 011002 (2013).

[26] G. Kresse and J. Hafner, “*Ab Initio* molecular dynamics for liquid metals,” Phys. Rev. B **47**, 558–561 (1993).

[27] G. Kresse and J. Furthmüller, “Efficiency of ab-initio total energy calculations for metals and semiconductors using a plane-wave basis set,” Comput. Mat. Sci. **6**, 15–50 (1996).

[28] G. Kresse and J. Furthmüller, “Efficient iterative schemes for *ab initio* total-energy calculations using a plane-wave basis set,” Phys. Rev. B **54**, 11169–11186 (1996).

[29] M. Gajdoš, K. Hummer, G. Kresse, J. Furthmüller, and F. Bechstedt, “Linear optical properties in the projector-augmented wave methodology,” Phys. Rev. B **73**, 045112 (2006).

[30] K. Berland and P. Hyldgaard, “Exchange functional that tests the robustness of the plasmon description of the van der Waals density functional,” Phys. Rev. B **89** (2014).

[31] K. Berland, V. R. Cooper, K. Lee, E. Schröder, T. Thonhauser, P. Hyldgaard, and B. I. Lundqvist, “Van der Waals forces in density functional theory: A review of the vdW-DF method,” Rep. Prog. Phys. **78**, 066501 (2015).

[32] D. O. Lindroth and P. Erhart, “Thermal transport in van der Waals solids from first-principles calculations,” Phys. Rev. B **94**, 115205 (2016).

[33] L. Gharaee, P. Erhart, and P. Hyldgaard, “Finite-temperature properties of nonmagnetic transition metals: Comparison of the performance of constraint-based semilocal and nonlocal functionals,” Phys. Rev. B **95** (2017), 10.1103/PhysRevB.95.085147.

[34] P. Hyldgaard, Y. Jiao, and V. Shukla, “Screening nature of the van der Waals density functional method: A review and analysis of the many-body physics foundation,” J. Phys. Condens. Matter

(2020).

[35] A. V. Krukau, O. A. Vydrov, A. F. Izmaylov, and G. E. Scuseria, "Influence of the exchange screening parameter on the performance of screened hybrid functionals," J. Chem. Phys. **125**, 224106 (2006).

[36] G. K. Madsen and D. J. Singh, "BoltzTraP. A code for calculating band-structure dependent quantities," Comput. Phys. Commun. **175**, 67–71 (2006).

[37] K. Berland and C. Persson, "Enabling accurate first-principle calculations of electronic properties with a corrected k · p scheme," Comput. Mater. Sci. **134**, 17–24 (2017).

[38] K. Berland and C. Persson, "Thermoelectric transport of GaAs, InP, and PbTe: Hybrid functional with k.p interpolation versus scissor-corrected generalized gradient approximation," J. App. Phys. **123**, 205703 (2018).

[39] K. Berland, N. Shulumba, O. Hellman, C. Persson, and O. M. Løvvik, "Thermoelectric transport trends in group 4 half-Heusler alloys," J. App. Phys. **126**, 145102 (2019).

[40] O. Hellman, I. A. Abrikosov, and S. I. Simak, "Lattice dynamics of anharmonic solids from first principles," Phys. Rev. B **84**, 180301 (2011).

[41] O. Hellman and D. A. Broido, "Phonon thermal transport in bi$_2$te$_3$ from first principles," Phys. Rev. B **90**, 134309 (2014).

[42] N. Shulumba, O. Hellman, and A. J. Minnich, "Lattice Thermal Conductivity of Polyethylene Molecular Crystals from First-Principles Including Nuclear Quantum Effects," Phys. Rev. Letters **119** (2017).

[43] J. P. Perdew, K. Burke, and M. Ernzerhof, "Generalized Gradient Approximation Made Simple," Phys. Rev. Lett. **77**, 3865–3868 (1996).

[44] J. He, M. Amsler, Y. Xia, S. S. Naghavi, V. I. Hegde, S. Hao, S. Goedecker, V. Ozoliņš, and C. Wolverton, "Ultralow Thermal Conductivity in Full Heusler Semiconductors," Phys. Rev. Lett. **117**, 046602 (2016).

[45] F. Zhou, W. Nielson, Y. Xia, and V. Ozoliņš, "Lattice anharmonicity and thermal conductivity from compressive sensing of first-principles calculations," Phys. Rev. Lett. **113**, 185501 (2014).

[46] Z. Feng, Y. Fu, Y. Zhang, and D. J. Singh, "Characterization of rattling in relation to thermal conductivity: Ordered half-Heusler semiconductors," Phys. Rev. B **101**, 064301 (2020).

[47] B. Abeles, "Lattice Thermal Conductivity of Disordered Semiconductor Alloys at High Temperatures," Phys. Rev. **131**, 1906–1911 (1963).

[48] Z. Tian, J. Garg, K. Esfarjani, T. Shiga, J. Shiomi, and G. Chen, "Phonon conduction in PbSe, PbTe, and PbTe$_{1-x}$Se$_x$ from first-principles calculations," Phys. Rev. B: Condens. Matter Mater. Phys. **85**, 184303 (2012).

[49] A. Katre, J. Carrete, and N. Mingo, "Unraveling the dominant phonon scattering mechanism in the thermoelectric compound ZrNiSn," J. Mater. Chem. A **4**, 15940 (2016).

[50] M. Arrigoni, J. Carrete, N. Mingo, and G. K. H. Madsen, "First-principles quantitative prediction of the lattice thermal conductivity in random semiconductor alloys: The role of force-constant disorder," Phys. Rev. B **98**, 115205 (2018).

[51] J. Carrete, N. Mingo, S. Wang, and S. Curtarolo, "Nanograined Half-Heusler Semiconductors as Advanced Thermoelectrics: An Ab Initio High-Throughput Statistical Study," Adv. Func. Mater. **24**, 7427–7432 (2014).

[52] W. Li, L. Lindsay, D. A. Broido, D. A. Stewart, and N. Mingo, "Thermal conductivity of bulk and nanowire Mg$_2$Si$_x$Sn$_{1-x}$ alloys from first principles," Phys. Rev. B **86**, 174307 (2012).

[53] S. N. H. Eliassen, A. Katre, G. K. H. Madsen, C. Persson, O. M. Løvvik, and K. Berland, "Lattice thermal conductivity of Ti$_x$Zr$_y$Hf$_{1\text{-x-y}}$NiSn half-Heusler alloys calculated from first principles: Key role of nature of phonon modes," Phys. Rev. B **95**, 045202 (2017).

[54] M. Schrade, K. Berland, S. N. H. Eliassen, M. N. Guzik, C. Echevarria-Bonet, M. H. Sørby, P. Jenus, B. C. Hauback, R. Tofan, A. E. Gunnæs, C. Persson, O. M. Løvvik, and T. G. Finstad, "The role of grain boundary scattering in reducing the thermal conductivity of polycrystalline XNiSn (X = Hf, Zr, Ti) half-Heusler alloys," Sci. Rep. **7** (2017).

[55] D. I. Bilc, G. Hautier, D. Waroquiers, G.-M. Rignanese, and P. Ghosez, "Low-Dimensional Transport and Large Thermoelectric Power Factors in Bulk Semiconductors by Band Engineering of Highly Directional Electronic States," Phys. Rev. Lett. **114**, 136601 (2015).

[56] M. Mikami, Y. Kinemuchi, K. Ozaki, Y. Terazawa, and T. Takeuchi, "Thermoelectric properties of tungsten-substituted heusler Fe$_2$VAl alloy," J. App. Phys. **111**, 093710 (2012).

[57] M. Vasundhara, V. Srinivas, and V. V. Rao, "Electronic transport in heusler-type Fe$_2$VAl$_{1-x}M_x$ alloys ($M = $ B, In, Si)," Phys. Rev. B **77**, 224415 (2008).

[58] D. Stoiber, M. Bobnar, P. Höhn, and R. Niewa, "Lithium alkaline earth tetrelides of the type Li2AeTt (Ae=Ca, Ba, Tt=Si, Ge, Sn, Pb): Synthesis, crystal structures and physical properties," Z. Naturforsch. B **72**, 847–853 (2017).

[59] J. Park, Y. Xia, and V. Ozoliņš, "High Thermoelectric Power Factor and Efficiency from a Highly Dispersive Band in Ba 2 Bi Au," **11**, 014058 (2019).

[60] G. D. Mahan and J. O. Sofo, "The best thermoelectric." PNAS **93**, 7436–7439 (1996).

[61] J. He, Y. Xia, S. S. Naghavi, V. Ozoliņš, and C. Wolverton, "Designing chemical analogs to PbTe with intrinsic high band degeneracy and low lattice thermal conductivity," Nat. Commun. **10**, 719 (2019).

[62] J. Zhou, H. Zhu, T.-H. Liu, Q. Song, R. He, J. Mao, Z. Liu, W. Ren, B. Liao, D. J. Singh, Z. Ren, and G. Chen, "Large thermoelectric power factor from crystal symmetry-protected non-bonding orbital in half-Heuslers," Nature Communications **9**, 1721 (2018).

[63] M. Zahedifar and P. Kratzer, "Band structure and thermoelectric properties of half-Heusler semiconductors from many-body perturbation theory," Phys. Rev. B **97**, 035204 (2018).

[64] J. R. Sootsman, R. J. Pcionek, H. Kong, C. Uher, and M. G. Kanatzidis, "Strong Reduction of Thermal Conductivity in Nanostructured PbTe Prepared by Matrix Encapsulation," Chem. Mater. **18**, 4993–4995 (2006).

[65] O. Delaire, J. Ma, K. Marty, A. F. May, M. A. McGuire, M.-H. Du, D. J. Singh, A. Podlesnyak, G. Ehlers, M. D. Lumsden, and B. C. Sales, "Giant anharmonic phonon scattering in PbTe," Nat. Mater. **10**, 614–619 (2011).

[66] M. K. Jana, K. Pal, U. V. Waghmare, and K. Biswas, "The Origin of Ultralow Thermal Conductivity in InTe: Lone-Pair-Induced Anharmonic Rattling," Angew. Chem. Int. Ed. **55**, 7792–7796 (2016).

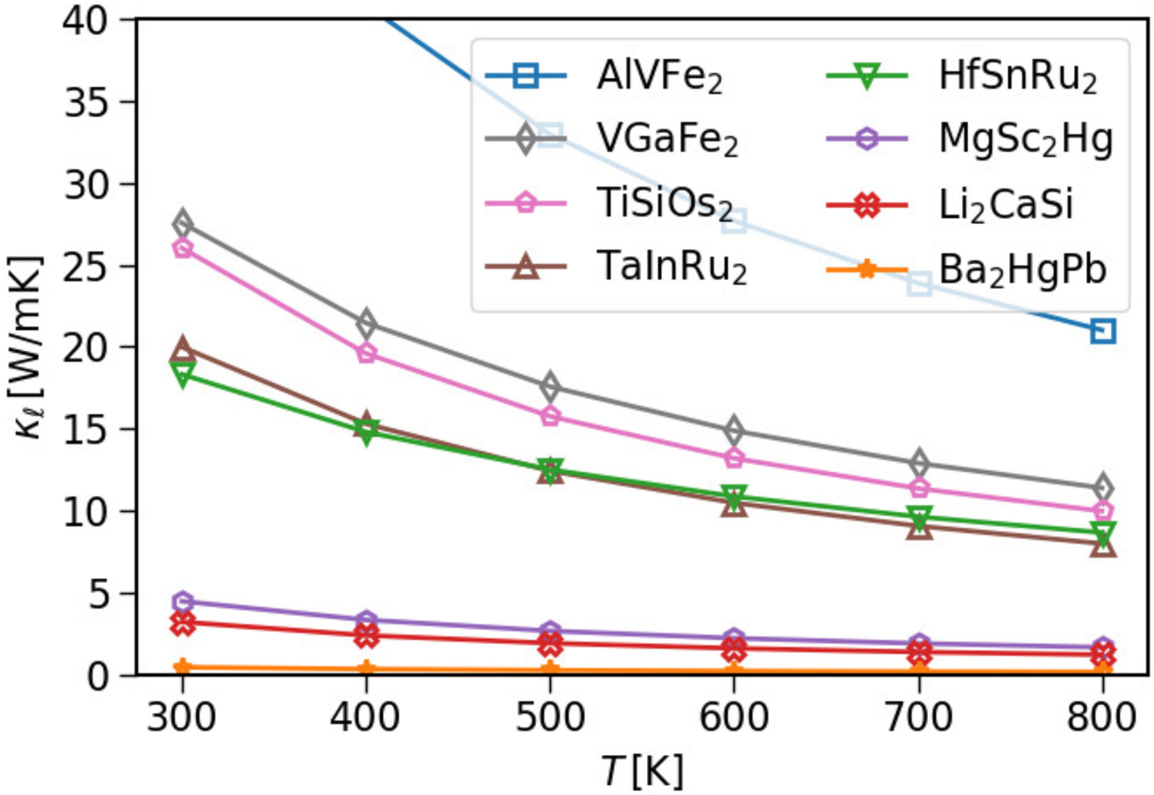
κ_ℓ [W/mK]
40
35
30
25
20
15
10
5
0
300
400
500
600
700
800
T [K]
AlVFe$_2$
VGaFe$_2$
TiSiOs$_2$
TaInRu$_2$
HfSnRu$_2$
MgSc$_2$Hg
Li$_2$CaSi
Ba$_2$HgPb

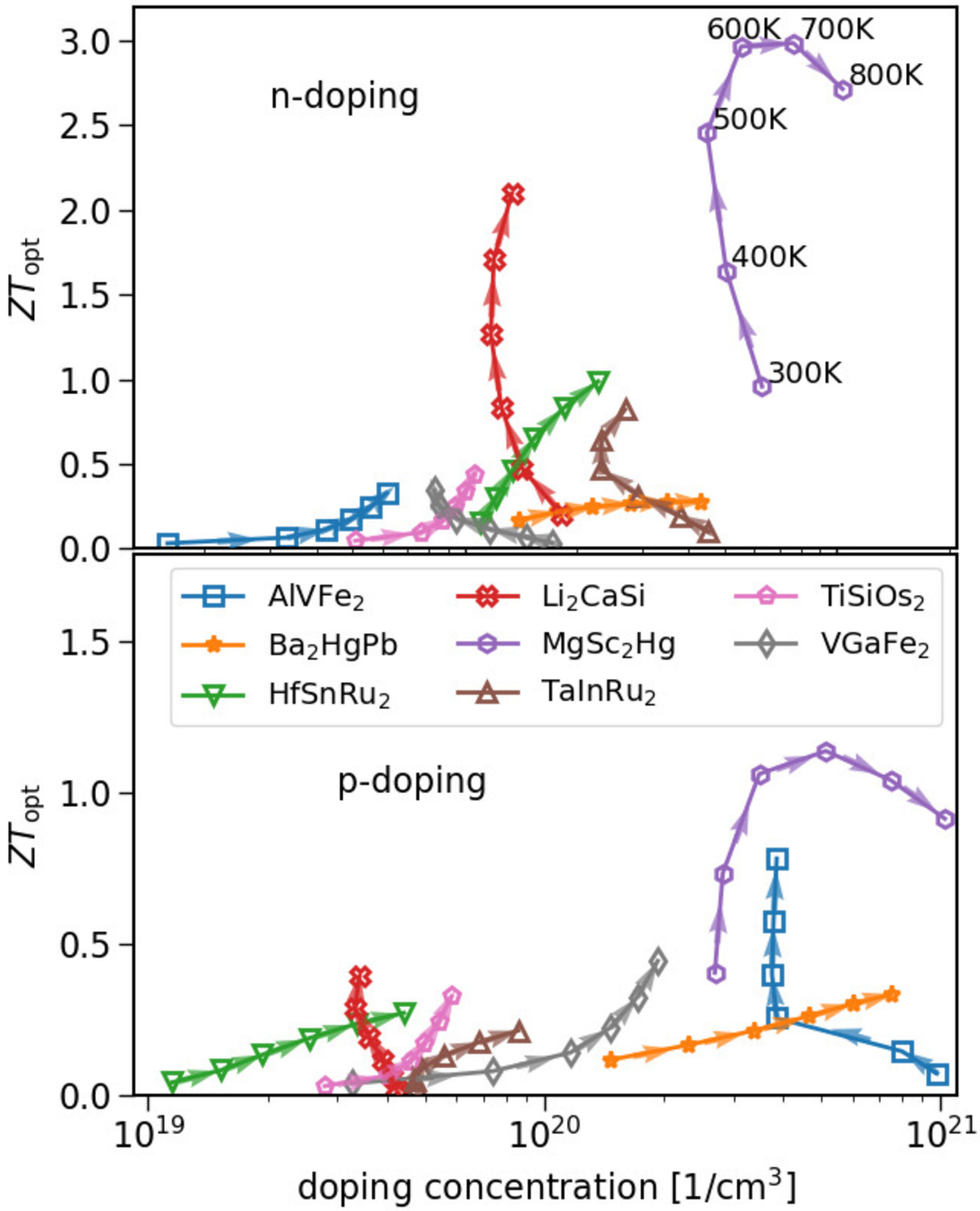
n-doping
600K
700K
800K
500K
400K
300K
ZT_{opt}
3.0
2.5
2.0
1.5
1.0
0.5
0.0
AlVFe$_2$
Li$_2$CaSi
TiSiOs$_2$
Ba$_2$HgPb
MgSc$_2$Hg
VGaFe$_2$
HfSnRu$_2$
TaInRu$_2$
p-doping
ZT_{opt}
1.5
1.0
0.5
0.0
10^{19}
10^{20}
10^{21}
doping concentration [1/cm^3]

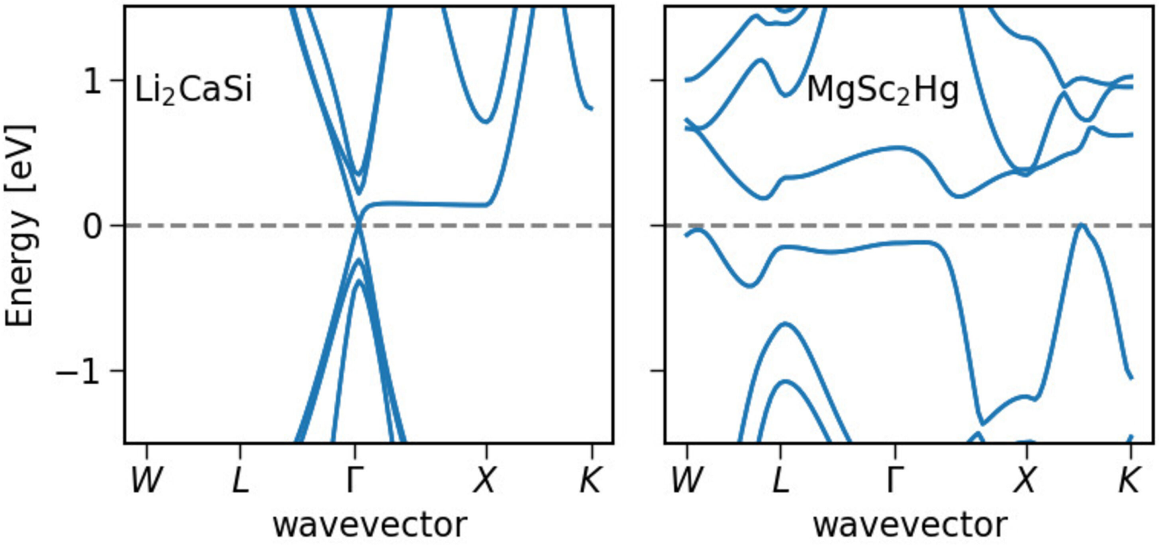
Li$_2$CaSi
MgSc$_2$Hg
Energy [eV]
1
0
−1
W
L
Γ
X
K
wavevector

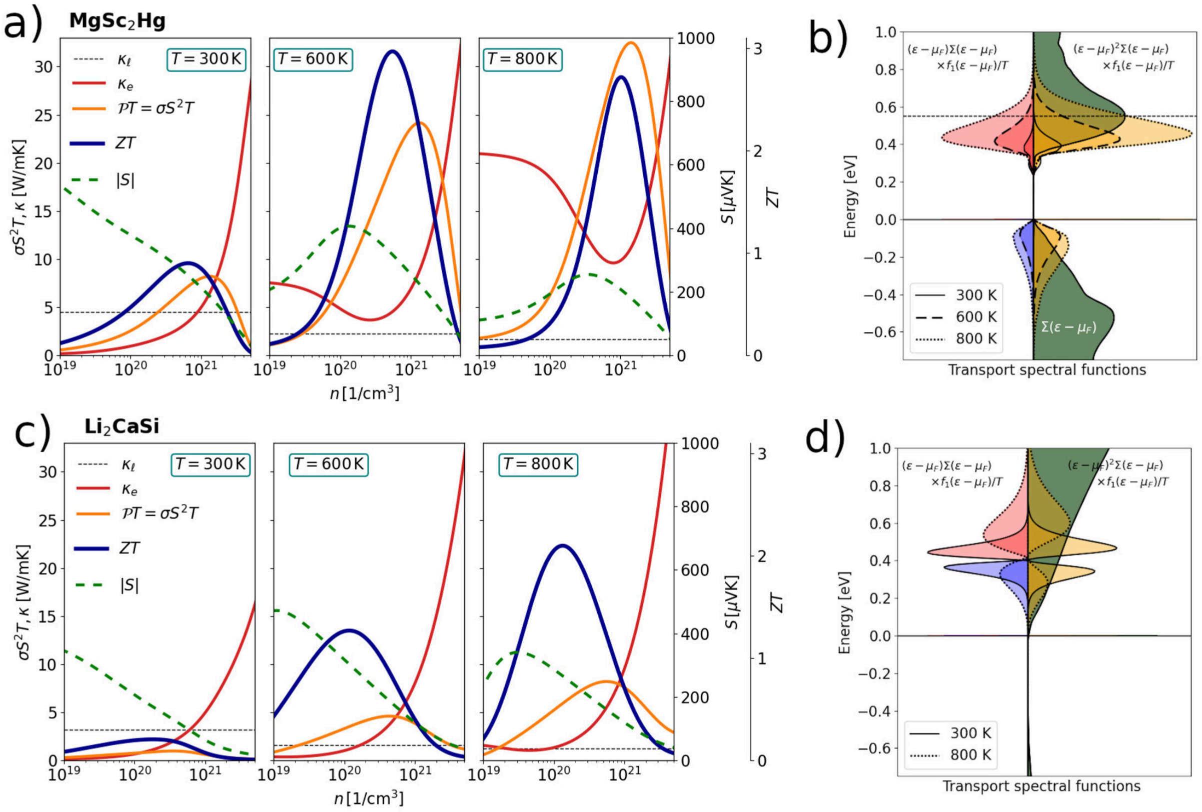
a)
MgSc$_2$Hg
κ_ℓ
κ_e
$\mathcal{P}T = \sigma S^2 T$
ZT
$|S|$
$T = 300$ K
$T = 600$ K
$T = 800$ K
$\sigma S^2 T, \kappa$ [W/mK]
$S\,[\mu$V/K]
ZT
n [1/cm^3]
b)
$(\varepsilon - \mu_F)\Sigma(\varepsilon - \mu_F)$
$\times f_1(\varepsilon - \mu_F)/T$
$(\varepsilon - \mu_F)^2\Sigma(\varepsilon - \mu_F)$
$\times f_1(\varepsilon - \mu_F)/T$
$\Sigma(\varepsilon - \mu_F)$
300 K
600 K
800 K
Energy [eV]
Transport spectral functions
c)
Li$_2$CaSi
κ_ℓ
κ_e
$\mathcal{P}T = \sigma S^2 T$
ZT
$|S|$
$T = 300$ K
$T = 600$ K
$T = 800$ K
$\sigma S^2 T, \kappa$ [W/mK]
$S\,[\mu$V/K]
ZT
n [1/cm^3]
d)
$(\varepsilon - \mu_F)\Sigma(\varepsilon - \mu_F)$
$\times f_1(\varepsilon - \mu_F)/T$
$(\varepsilon - \mu_F)^2\Sigma(\varepsilon - \mu_F)$
$\times f_1(\varepsilon - \mu_F)/T$
300 K
800 K
Energy [eV]
Transport spectral functions